PBM and Activated Sludge Flocculation: From Experimental Data to Calibrated Model

I. Nopens, T. Koegst, K. Mahieu, and P. A. Vanrolleghem
Biomath, Ghent University, Coupure Links 653, B-9000 Ghent, Belgium

DOI 10.1002/aic.10402
Published online March 23, 2005 in Wiley InterScience (www.interscience.wiley.com).

A new comprehensive calibration methodology for a population balance model (PBM) is presented using experimental size distribution data obtained on-line during flocculation tests. It was found that the moving-pivot discretization technique should be used to accurately solve the PBM. A new methodology for grid transformation and volume to number transformation, based on the sludge concentration and the densities of liquid, solids, and flocs, is presented. Model fits were performed on four different fitting variables. Volume-based fitting (vol % and D[4, 3]) tends to fit the middle part of both the vol % and number distribution better than the tails of smaller and larger particle sizes. Severe underpredictions (up to a factor of 30) of the lower-size classes are observed at steady state. Number-based fitting [(weighted) number distribution] tends to fit the small-size classes better, but still underpredicts them by a factor of 2 at steady state. © 2005 American Institute of Chemical Engineers *AIChE J,* 51: 1548–1557, 2005
Keywords: population balance, parameter identification, optimization, sedimentation, calibration, activated sludge

Introduction

The activated sludge process is a widely used biological process in wastewater treatment. It can roughly be divided into two steps: purification of the wastewater and liquid–solid separation. During the first step the organic loading [chemical oxygen demand (COD)] and nutrients (N and P) are, to a certain extent, removed from the wastewater to meet effluent standards. This process can occur in a variety of configurations combining aerobic, anoxic, and anaerobic zones and has been thoroughly studied.[1] The second step deals with the separation of the purified water and the sludge flocs. Compared to the first step, this process is much less understood and is still a frequently occurring bottleneck in the overall performance of the activated sludge process. Indeed, faulty clarification results, on the one hand, in a loss of biomass (which contains nutrients and COD) by the overflow, which deteriorates the effluent quality. On the other hand, the overall removal efficiency of the plant deteriorates, given that biomass that is capable of purifying the incoming wastewater is lost from the system. Because of this lack of knowledge, simple one-dimensional models are often used to approximately describe the final clarification step when attempting to model the entire activated sludge process (purification + separation). More accurate and knowledge-based models to describe the separation step are needed to achieve overall model predictions.

Liquid–solid separation in the final clarifier mainly depends on clarifier hydrodynamics and activated sludge properties. The former attempts to describe influences such as inlet construction, tank geometry, baffle location, and loading rate, and is commonly tackled by means of computational fluid dynamics (CFD).[2-5] CFD aims at modeling the fluid dynamics of the clarifier by using continuity, momentum, and turbulence equations. This allows prediction of velocity and sludge concentration profiles for the complete clarifier both in space and time. Current CFD models, however, do not account for flocculation of the solids, leading not only to inaccurate predictions of the sludge concentration profile in the clarifier (when compared to experimental data) but also to inaccurate predictions of the suspended solids concentration in the effluent, which is one of

Correspondence concerning this article should be addressed to I. Nopens at Ingmar@biomath.ugent.be.

the aims of these models.[5] Despite much effort, the activated sludge flocculation process is still poorly understood and thus no model is yet available that accurately describes the process. Flocculation depends not only on floc properties, such as floc size distribution (FSD) and floc structure (both microbiological and physical), but also on local flocculation conditions, including shear forces induced by the flow regime, sludge concentration, and ionic strength. Detailed information about the activated sludge flocculation process needs to be gathered and included in the CFD model to achieve a good overall description of settling tank performance.

One of the main reasons for the poor understanding of the activated sludge flocculation process is the difficulty of monitoring it on-line. To date, on-line studies dealing with activated sludge flocculation are rather scarce, compared to their non-biological counterparts. During the last few decades, different techniques have been developed that facilitate measurement of particle size distributions, although all have their drawbacks.[6] Alternative measurements such as supernatant turbidity, settling velocity, and sludge volume index (SVI)[7-9] have been applied. However, these variables are unable to describe the detailed interactions occurring in the activated sludge flocculation process. Other techniques that are able to quickly provide quantitative information about the flocculation process are light-scattering techniques such as laser rotation and laser-light diffraction. The first technique was successfully applied to monitor particle aggregation and breakup of inorganic particles in a shear flow,[10] whereas the latter has been applied to characterize the floc structure.[11,12] It can also be applied to monitor changes in floc size distribution as flocculation proceeds.[9,13]

Recently, a laser-diffraction technique was used to provide the experimental data to which a population balance model (PBM) was fitted by estimating the aggregation and breakage parameters of sludge flocs.[6,13]

The current paper introduces a considerably improved overall methodology to calibrate a PBM for sludge flocculation based on experimental size distribution data obtained on-line during flocculation.

The Population Balance Model

The aforementioned activated sludge models and also simple one-dimensional settling models use a lumped variable to describe the biomass: the activated sludge concentration X. However, to allow for description of processes including interactions between individuals of a population (in this case flocculation of sludge flocs), another way of describing the biomass is needed: a so-called segregated model. This type of model *segregates* the population (= biomass) into individual entities (sludge flocs). This approach implies that all individual properties of the flocs are also segregated and will result in property distributions instead of a single average quantity for a certain property. Models describing the time evolution of these property distributions are commonly known as *population balance models* and have been successfully applied to describe processes such as crystallization,[14] flocculation of inorganic dispersed systems,[15] polymerization,[16] precipitation,[17] flotation,[18] granulation,[19] cell culture dynamics,[20] and aerosol dynamics,[21] to identify but a few. Depending on the number of properties being described, a PBM can be categorized as either

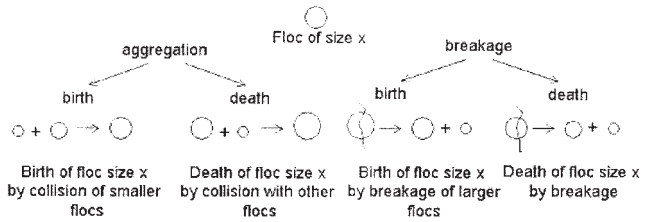

Figure 1. Aggregation and breakage dynamics of the discretized population balance.[41]

one- or multidimensional. The general format of a one-dimensional PBM is expressed as[22,23]

$$\frac{\partial n(x,\,t)}{\partial t} + \frac{\partial}{\partial x}\left[\dot{X}(x,\,t)n(x,\,t)\right] = h(x,\,t) \tag{1}$$

where x is a property of the individuals, $n(x, t)$ is the number-based property distribution function (m^{-3}), $\dot{X}(x, t)$ is the time derivative of the property x (s^{-1}), and $h(x, t)$ is the net aggregation rate ($m^{-3}\ s^{-1}$). In the application at hand, x is chosen to be the floc size (expressed as volume) and thus Eq. 1 describes the time evolution of the number-based floc size distribution. $\dot{X}(x, t)$ can be interpreted as the bacterial growth rate. Because the model will be used to describe rather short flocculation experiments (max. 14.4E+3 s), it can be assumed that no significant growth occurs, allowing omission of the second term on the left-hand side of Eq. 1. $h(x, t)$ accounts for discontinuous aggregation/breakage processes (Figure 1). It describes the creation or *birth* and the disappearance or *death* of flocs of a certain size x during an infinitesimal time interval δt. Because both aggregation and breakage can give rise to birth and death of flocs, $h(x, t)$ consists of four processes: aggregation birth (AB), aggregation death (AD), breakage birth (BB), and breakage death (BD), illustrated in the following equation

$$h(x,\,t) = h(x,\,t)_{agg} + h(x,\,t)_{break} = h(x,\,t)_{AB} - h(x,\,t)_{AD} + h(x,\,t)_{BB} - h(x,\,t)_{BD} \tag{2}$$

Aggregation models are often based on the Smoluchowski model[23,24]

$$h(x,\,t)_{agg} = \frac{1}{2}\int_0^x \alpha\beta(x-x',\,x')n(x-x',\,t)n(x',\,t)dx' - n(x,\,t)\int_0^\infty \alpha\beta(x,\,x')n(x',\,t)dx' \tag{3}$$

where $\beta(x, x')$ ($m^3\ s^{-1}$) is the collision frequency for particles of volume x (m^3) and x' (m^3) and α is the collision efficiency. The former describes the transport of flocs toward one another, whereas the latter expresses the probability that these collisions lead to aggregation, taking into account short-range forces such as van der Waals interaction, electrostatic repulsion, and hydrodynamic interaction. The description of $\beta(x - x', x)$ used in this study was taken from[15]

$$\beta(x - x', x) = 0.31\bar{G}[x^{1/3} + (x - x')^{1/3}]^3 \quad (4)$$

in which

$$\bar{G} = \left(\frac{\bar{\varepsilon}}{\nu}\right)^{1/2} \quad (5)$$

where $\bar{G}$ is the average velocity gradient (s^{-1}), ν is the kinematic viscosity ($m^2\ s^{-1}$), and $\bar{\varepsilon}$ is the average turbulent energy dissipation rate ($m^2\ s^{-3}$); α was chosen to be a constant between 0 and 1. In the latter case, all collisions are considered to be successful. Other aggregation models are available in literature.[25-27]

Breakage models typically have the following format[23]

$$h(x, t)_{break} = \int_x^\infty n(x', t)S(x')\Gamma(x|x')dx' - n(x, t)S(x)\Gamma(x|x') \quad (6)$$

where $S(x)$ is the breakage rate of particles of size x (s^{-1}); and $\Gamma(x|x')$ is the breakage distribution function, expressing the probability that a particle of volume x will be formed from the breakage of a particle with volume x'. $S(x)$ was taken from[15]

$$S(x) = Ax^a \quad (7)$$

where a is a constant ($=1/3$) and A is the breakage rate coefficient ($m^{-1}\ s^{-1}$). This expresses that the breakage rate is proportional to the diameter of the floc (x is expressed as volume). When binary breakage into equally sized daughters is assumed (which was the case in this study), $\Gamma = 2$ for successive classes (in the case of a geometric grid with factor of 2). Other, more complex breakage functions can be found in the literature.[27-30]

Equations 1–7 describe the PBM used in this study. As can be observed from Eqs. 3 and 6, the birth and death terms are typically integral functions containing $n(x, t)$ in the integrandum, making Eq. 1 a so-called integrodifferential equation. This type of equation rarely has an analytical solution [depending on the complexity of $h(x, t)$]. A number of solution methods have been described.[23] When a fast solution is required (such as parameter estimation, control, PBM in combination with CFD, and the like), discretization of the population property has proven to be useful. Moreover, these methods are relatively easy to implement in simulation platforms that already contain a numerical integrator. Therefore, other solution methods were not considered at this stage of the research. The discretization approach, which has received quite some attention in the literature,[29,31-34] divides the property range in a finite number of classes (M), transforming the integrodifferential equation into a set of M ordinary differential equations that can be solved simultaneously. Several discretization schemes exist, mainly differing in terms of (1) freedom to choose the discretization grid and (2) conserved properties (at least two) during the discretization.[35] Kumar and Ramkrishna proposed two general techniques: the fixed pivot[32] and the moving pivot,[33] where the *pivot* is the representative diameter of a size class. The techniques are general with respect to grid choice and do not require reformulation of the algorithm when other properties need to be conserved, which is the case when using other methods.[31,34]

Materials and Methods

Experimental setup

The experimental data used in this study were obtained from Biggs and Lant,[13] who were the first researchers to study the influence of mixing intensity and calcium addition on flocculation kinetics on-line. Before the experiments, the sludge flocs were sonicated to deflocculate them into single cells (1E-6 m) and microcolonies of about 1E-5 m. The sonication time was chosen in a way so as not to cause significant cell lysis. The sludge was then allowed to reflocculate under certain specific conditions of mixing intensity and calcium addition and was circulated through a Mastersizer E (Malvern Instruments, Malvern, U.K.) to obtain on-line quantitative information about floc structure, floc size distribution (FSD), and their derived equivalent diameters. The measurement technique is based on forward laser-light diffraction and has been used by other researchers.[9,11-13,15,36] The sludge flocs are brought in a laser beam, where they cause forward scattering of the incoming light. Small particles will scatter the light in the large-angle range, whereas large particles scatter the light in the small-angle range. Thus, a heterogeneous particle population will result in a diffraction pattern. This light intensity pattern is measured by a number of detectors located at different angles. An optical model (such as Mie or Fraunhofer) is then used to transform the diffraction pattern into an FSD. The latter is presented as a volume percentage (vol %) distribution (that is, the percentage of total solids volume in every size class), but other descriptive parameters can be derived from it such as different integral moments and weighted diameters such as the mass mean diameter (also termed $D[4, 3]$), defined as the ratio of the fourth and third moment of the distribution (in its discrete form)

$$D[4, 3] = \frac{\sum_{i=1}^n \Delta F_N(d)_i d_i^4}{\sum_{i=1}^n \Delta F_N(d)_i d_i^3} \quad (8)$$

where d_i represents the diameter of size class i (m) and $\Delta F_N(d)_i$ is the number fraction in size class i ($=N_i/\sum N_i$).

The main advantage of this technique is the on-line applicability. Drawbacks of the laser-diffraction method are: (1) the assumption of sphericity of particles in the optical model, and (2) the required dilution step ($<0.2\ kg\ m^{-3}$) to avoid multiple scattering because this is not taken into account by the optical model. The latter is checked by means of the obscuration level, which should be inside a certain range. So as not to disturb the sample to be measured by, for instance, a change in ionic strength, filtered effluent (4.5 E-7 m) should be used for dilution purposes.[37] The flow rate to the flow-through cell was determined in such a way as to minimize shear effects and pump pulsation influences and to avoid settling in the tubes (to approximate isokinetic sampling). A flow rate of 3E-3 kg s^{-1} was selected.[13]

Numerical methods

To solve the PBM, two different discretization techniques were used: the fixed-pivot[32] and the moving-pivot techniques,[33] both of which allow a free choice of grid. In this discretized size range only particles of these pivotal sizes exist. However, aggregation and/or breakage processes give rise to particles of other, nonexisting sizes. The fixed-pivot technique redistributes these particles to the adjoining pivots. The number of pivots to which the particles are redistributed determines the number of properties that can be conserved by the algorithm. Typically, it is chosen to redistribute mass and numbers to the two adjoining pivots. In the moving-pivot case, the pivot is allowed to move within the boundaries of the class it represents. This establishes a more accurate algorithm, although it requires additional equations to describe the movement of the pivots. For a more detailed explanation, the reader is referred to the literature.[32,33,35]

Both algorithms were implemented in the modeling and simulation software platform WEST (Hemmis NV, Kortrijk, Belgium).

Optimizations were conducted using either a least-squares (LS) or a weighted least-squares (WLS) method[38]

$$J(\theta) = \sum_{i=1}^{N} [y_i - \hat{y}_i(\theta)]^2 \qquad \text{LS} \tag{9}$$

$$J(\theta) = \sum_{i=1}^{N} \frac{1}{\sigma_i^2} [y_i - \hat{y}_i(\theta)]^2 \qquad \text{WLS} \tag{10}$$

where $J(\theta)$ is the so-called sum of squared errors (SSE) or objective function; y_i is the experimental variable; $\hat{y}_i(\theta)$ is the model prediction using parameter set θ; N is the number of experimental data points; and $1/\sigma_i^2$ is the weight for measurement i, often taken to be the inverse of the measurement error. The simplex optimization algorithm[39] was used to minimize $J(\theta)$. If one wants to fit simultaneously to different variables (experimental data sets), Eqs. 9 and 10, respectively, become

$$J(\theta) = \sum_{j=1}^{m} \sum_{i=1}^{N_j} [y_{i,j} - \hat{y}_{i,j}(\theta)]^2 \qquad \text{LS} \tag{11}$$

$$J(\theta) = \sum_{j=1}^{m} \sum_{i=1}^{N_j} \frac{1}{\sigma_{i,j}^2} [y_{i,j} - \hat{y}_{i,j}(\theta)]^2 \qquad \text{WLS} \tag{12}$$

where m is the number of experimental data sets and N_j is the number of experimental datapoints of the jth experiment.

Results and Discussion

The goal of this work is to introduce a new comprehensive calibration methodology for PBM using experimentally collected flocculation data. It discusses problems that arise during a calibration procedure and will influence the results, such as (1) the choice of solution method (in this case discretization methods were used), (2) data transformations that are necessary to be able to solve the discretized set of equations (3) measurement errors and (4) the choice of fitting variable.

Solution method

When calibrating a model using experimental data, it is important to use a relatively fast solution method (such as discretization techniques) because many simulations might be needed. In their work, Biggs and Lant[13] used the discretization technique of Hounslow et al.,[31] which is exactly the same as the fixed-pivot technique when using a geometric grid with factor 2 (such as 1, 2, 4, 8, . . . , E-18 m^3) and conserving both numbers (zeroth moment) and mass (third moment) during the discretization procedure. Kumar and Ramkrishna,[33] however, compared this fixed-pivot technique with an analytical solution for a simple PBM and found that it suffers from overpredictions of numbers when large gradients are present in the distribution. To deal with this, they introduced an alternative technique, the moving pivot, and showed that this technique gave a much better prediction of the analytical solution, even for a coarse grid. To confirm this improved accuracy in this study, the PBM was solved with both techniques, fixed and moving pivots, using the same parameter set (α = 6.5E-3 and A = 201.5 m^{-1} s^{-1}). The simulation results are represented as cumulative oversize numbers (CON)

$$\text{CON}(x, t) = \int_x^{\infty} n(x', t)dx' \tag{13}$$

to emphasize the predictions of the large floc size tail and the zeroth moment (= total number of particles in the system) of the distribution in one single plot. It can be seen that the predictions of the fixed pivot starting from the same initial distribution (Figure 2A) indeed yields a lower zeroth moment (= total number of flocs) and a larger number of flocs in larger-size classes (Figure 2B), meaning that the aggregation has occurred faster compared to that of the moving pivot.

Also, the model solved with the different solution techniques was fitted to one of the experimental D[4, 3] data sets of Biggs and Lant[13] using the LS objective function (Eq. 9). The resulting parameter values are given in Table 1. It can be observed that the estimate of parameter α is much lower when the fixed pivot is used because the technique inherently speeds up the aggregation. To fit the same data set, the aggregation parameter α must be decreased (by 50%), leading to erroneous parameter estimates. The difference in A is less pronounced, as was previously observed by Nopens and Vanrolleghem.[35]

Corroborating the conclusions by Kumar and Ramkrishna,[33] it is therefore advisable to use the moving pivot to solve the PBM to obtain accurate estimates of α and A.

Data transformation

Every transformation of experimentally collected data will unavoidably introduce some error and should be minimized. In some cases, however, transformations cannot be avoided because of incompatibility of the model and the experimental data, as was the case in this study.

The raw output of the Mastersizer is a vol % distribution for a given grid, based on which the number distribution and some

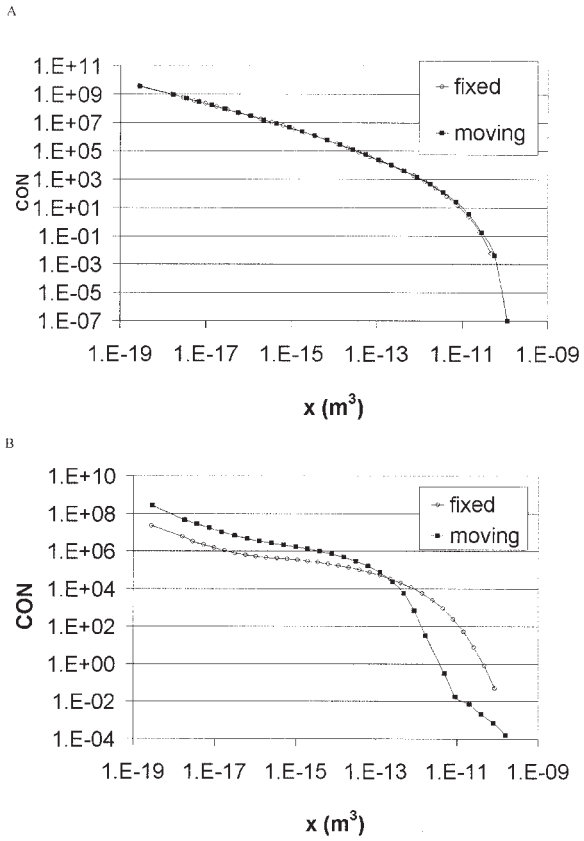

Figure 2. Difference between fixed and moving pivot solutions at (A) $t = 0$ and at (B) $t = 2000$ s.

summarizing parameters are calculated. On the other hand, the model is formulated on a number basis and uses a different grid. Thus, recalculation of the experimental Malvern data is required to make them compatible with the model grid (geometric with a factor of 2). Moreover, a volume-to-number conversion is needed to obtain an initial distribution to supply the model.

Prompted by conclusions reported in the literature,[40] Biggs and Lant[13] fitted lognormal distributions to the original raw vol % distributions. The fits were claimed to be good based on high correlation coefficients ($R^2 \cong 0.92$), although clear deviations can be observed near the tails of the distribution. This is illustrated in Figure 3 by comparing the raw cumulative vol % distribution and the one calculated from the number distribution of Biggs and Lant.[13] These lognormal fits allowed interpolation of volume fractions along the entire floc size range. In

Table 1. Parameter Estimates of Fit on *D*[4, 3] Using Fixed and Moving Pivots on the Same Data Set ($G = 19.4\ s^{-1}$), and Parameters Found by Biggs and Lant for the Same Data Set (But Different Transformation)*

Parameter Estimate	α	A ($m^{-1}\ s^{-1}$)
Fixed	6.48E-3	202
Moving	1.36E-2	195
Biggs and Lant	4.95E-4	230

*Biggs and Lant.[13]

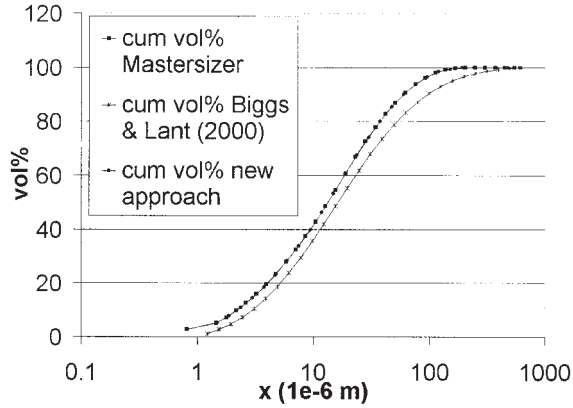

Figure 3. Comparison of original and recalculated cumulative vol %.

a second step the volume distribution was transformed into a number distribution, assuming the particles to be spherical.

Fitting the lognormal distributions as an intermediate step introduced large errors into the number distributions, even though high values of R^2 were obtained. Indeed, small deviations between the lognormal distribution and the experimental data increase substantially when number distributions are calculated. Biggs[41] reported this as a shift in *D*[4, 3] between that calculated from the raw data and that calculated from the transformed number distribution (Figure 4). Such differences are unacceptable and thus an alternative method is required. Parameter estimates found by Biggs and Lant[13] after fitting the model to this transformed *D*[4, 3] data set are reported in Table 1.

First, as an alternative approach to deal with the difference in the discretization grid, a cumulative vol % distribution is calculated from the raw distribution. The latter is then interpolated at the pivots of the new grid, resulting in a cumulative distribution in the new grid and allowing recalculation of the volume percentage distribution. Figures 3 and 4 show that this transformation does not alter the raw data.

Second, the incompatibility between the experimental vol % distributions and the number-based model needs to be solved. One could argue the need for this transformation and use a

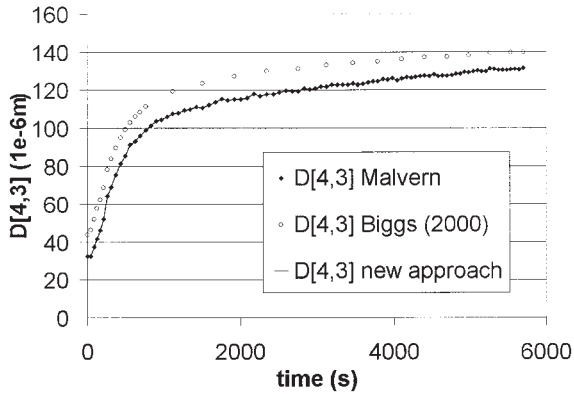

Figure 4. Difference between *D*[4, 3] based on (1) raw Mastersizer data, (2) the recalculated number distribution of Biggs,[41] and (3) the new approach.

volume-based model. However, this has two disadvantages: (1) it was illustrated before that fitting on volumes is dangerous because the tails often are under- or overpredicted, introducing severe errors; (2) the interpretation of the model is less clear when using a volume-based model. Instead of a number of particles N_i colliding with a number of particles N_j, a volume of particles v_i will collide with a volume of particles v_j, which is clearly more abstract and no longer compatible with Smoluchowski's law for aggregation.

The experimental data are expressed as vol % or the ratio between the floc volume in class i (V_i) and the total floc volume of all classes (V_f), V_i/V_f. The model, on the other hand, is expressed in number concentrations or the ratio between the number of particles of class i (N_i) and the total sample volume (V_T), N_i/V_T. To convert V_i into N_i, the total floc volume fraction V_f/V_T is needed.

Kinnear[42] derived a ratio (C) between the liquid and solid mass (m_l, m_s) within a sludge floc, based on the heterogeneous floc model and the densities of liquid (ρ_l), flocs (ρ_f), and dry solids (ρ_s)

$$C = \frac{m_l}{m_s} = \frac{\rho_l(\rho_s - \rho_l)}{\rho_s(\rho_f - \rho_l)} \tag{14}$$

Assuming that a floc consists of solids and interstitial bound water, a mass balance can be written as

$$m_f = m_s + m_l \tag{15}$$

Combining Eqs. 14 and 15 yields

$$m_f = (1 + C)m_s \tag{16}$$

Assuming constant densities for flocs and solids and dividing by the total sample volume V_T, one can rewrite Eq. 16 as

$$\frac{\rho_f V_f}{V_T} = (1 + C)\,\frac{\rho_s V_s}{V_T} \tag{17}$$

The second factor on the right-hand side of Eq. 17 is in fact the mixed liquor suspended solids (MLSS), which yields the following expression for the total volume of flocs

$$\frac{V_f}{V_T} = \frac{(1 + C)}{\rho_f} X = \frac{\rho_s - \rho_l}{\rho_s(\rho_f - \rho_l)} X \tag{18}$$

where X is the MLSS (kg m^{-3}). Equation 18 allows calculation of the total floc volume by using the measurements of MLSS and the floc, liquid, and dry solids densities. The former is a straightforward determination in wastewater treatment, whereas the latter can be obtained by means of density-gradient pycnometry.[42,43] Literature values for ρ_f range from 1010 to 1090 kg m^{-3}, whereas ρ_s ranges from 1200 to 1800 kg m^{-3}. As an example, the total floc volume for a sludge with $X = 3$ kg m^{-3}, and ρ_f, ρ_l, and ρ_s, respectively equal to 1040, 1000, and 1400 kg m^{-3}, was found to be 0.0214%. An overview of total floc volumes in different ranges of ρ_f and ρ_s and for MLSS = 3 kg m^{-3} is given in Figure 5. For a fixed ρ_f, the total floc volume increases when ρ_s increases. Heavier particles will cause the floc to contain more water to conserve the floc density, thus causing the floc to be more voluminous. For a fixed ρ_s, the total floc volume increases when ρ_f decreases. The latter could be expected, given that a floc with a smaller density (but identical solid density) needs to contain more water and will thus be more voluminous.

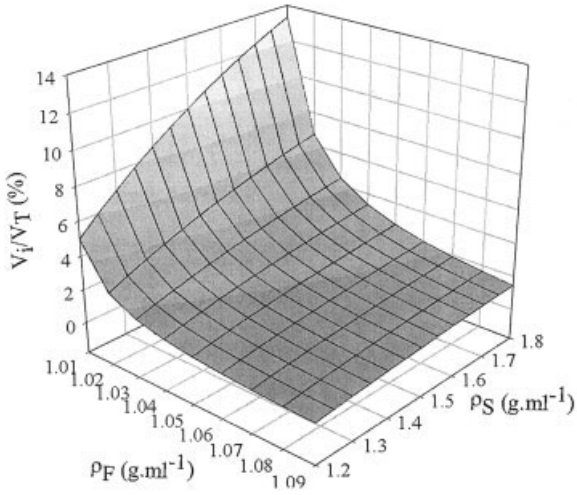

Figure 5. Total floc volumes calculated for different ranges of floc and dry solids densities ($X = 3$ g L^{-1}).

At this stage, the volume concentration and thus the number concentration can be calculated, assuming the flocs to be spherical

$$\frac{N_i}{V_T} = \left(\frac{6}{\pi d_i^3}\right)\frac{V_i}{V_f}\frac{V_f}{V_T} \tag{19}$$

where d_i is the diameter of a particle in size class i.

The D[4, 3] based on this new distribution exactly matches the one reported by the Mastersizer based on the raw volume percentage distribution (Figure 4). The parameter estimates reported in Table 1 for the fixed and moving pivots were obtained using this new conversion. Comparing them with the values found by Biggs and Lant,[13] it can be concluded that the new data conversion results in different parameters. In particular, the value of α is significantly higher and seems to be more realistic than the low value reported by Biggs and Lant.[13] This lower value can be explained by the fact that the system is, initially, in a more flocculated state and apparently does not require the same degree of flocculation to reach steady state (that is, smaller α).

Measurement errors

As mentioned earlier, measurement errors can be used in the WLS optimization procedure to account for the uncertainty of experimental data. Practically, this means that the discrepancies between model calculations and data with a high degree of uncertainty are less accounted for in the calculation of the WLS compared to data that have a lower degree of uncertainty.

In their work, Biggs and Lant[13] used only the mass mean diameter (D[4, 3]) as a fitting variable. Because the error was

assumed to be the same throughout the entire experiment, it was not used in a WLS. However, the measurement error value was used to calculate uncertainty intervals for the measurements to verify whether the model prediction was inside these intervals.

In this work, number distributions were also used as fitting variables. Because it is found that the measurement error is not the same for different size classes it is of interest to determine measurement errors for each size class. A similar approach using a repetition of measurements during a pseudo steady state cannot be applied here because the background flocculation cannot be quantified in each size class N_i. Because every FSD produced by the Mastersizer is determined by using a large number of measurements (or *sweeps*), one can assume every Mastersizer measurement to be a counting of particles in each size class N_i. Based on this assumption, every single measurement of N_i can be assumed to be multinomially distributed.[44] The variance of such a multinomial distribution represents the measurement error and can be calculated as follows[44]

$$\sigma^2(N_i) = N_i\left(1 - \frac{N_i}{N}\right) \tag{20}$$

where N is the total number of particles measured. This approach allows determination of the measurement errors for all size classes N_i from one single measurement.

Choice of fitting variable/parameter estimations

Two data sets were adopted from Biggs and Lant[13] and used to calibrate the PBM. They contain data of flocculation experiments at different mixing intensities represented by the average velocity gradient $\bar{G}$ (19.4 and 37.0 s^{-1}). The new approach based on the constant volume concentration was used for the conversion of raw vol % distributions to number distributions (using $X = 3$ kg m^{-3}, $\rho_l = 1000$ kg m^{-3}, $\rho_f = 1040$ kg m^{-3}, $\rho_s = 1700$ kg m^{-3}). The PBM was fitted to four different fitting variables using the entire range of experimental data: (1) volume percentage distributions, (2) $D[4, 3]$, (3) number distributions, and (4) weighted-number distributions. The parameter estimates of all optimizations are summarized in Table 2. Results of the predictions (for the case $\bar{G} = 19.4$ s^{-1}) of both the volume percentage distribution and the number distribution after a simulation time of 1920 s are given in Figure 6 for the four optimized cases. Similar results were found for $\bar{G} = 37.0$ s^{-1} (not shown). From the parameter estimates and the predictions of both the volume percentage and the number distribution, it can be seen that the choice of fitting variable is critical.

Table 2. Optimal Values for α and A for Different Mixing Intensities

Mixing Intensity G (s^{-1})	Fitting Variable	α	A (m^{-1} s^{-1})	$J(\theta)$
19.4	Vol %	1.21E-2	166	1336
	$D[4, 3]$	1.36E-2	195	2712
	N_i	7.3E-3	12	1.60E+19
	Weighted N_i	7.8E-3	12	2.64E+10
37.0	Vol %	8.30E-3	260	1926
	$D[4, 3]$	8.10E-3	260	1958
	N_i	9.80E-3	32	1.47E+19
	Weighted N_i	7.80E-3	18	3.76E+10

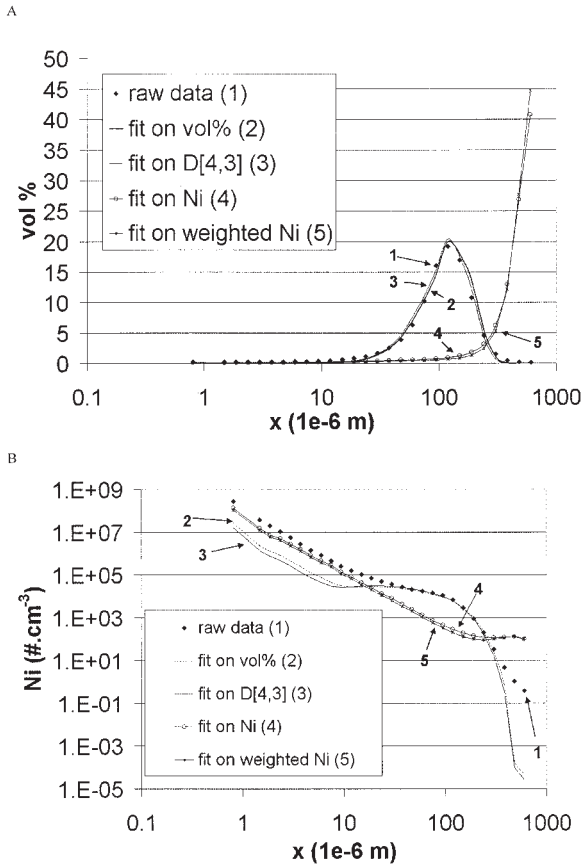

Figure 6. Comparison of model predictions at $t = 1920$ s of (A) the volume percentage distribution and (B) the number distribution after the model was fitted to different fitting variables.

On the other hand, both fits show that the model is not flexible enough and that the structure of the kernels needs to be investigated, although this is not the focus of the present study.

Fit on vol %/D[4, 3]. At first sight, fitting on the volume percentage distribution yields a fairly good result for the volume percentage distribution (Figure 6A). However, in sharper detail with respect to the tails of the distribution, it seems that both the lower and upper tail are underpredicted (Figure 7); the

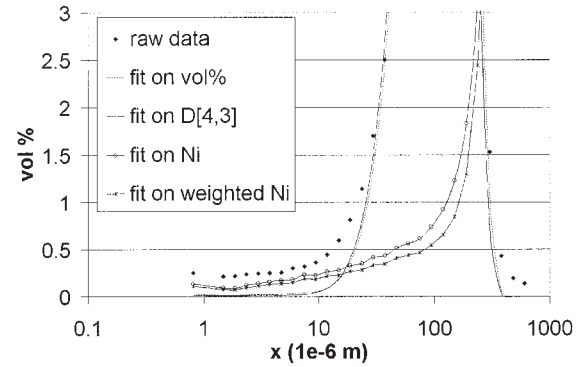

Figure 7. Close-up of plot of the small particle tail model predictions after the model was fitted to different fitting variables.

reason for this is merely the fact that the frequencies in these classes are low and will have a smaller contribution to the objective function [$J(\theta)$] in the LS optimization. For the application under study, the lower tail is of primary interest because flocs with these diameters will usually end up in the effluent. When looking at the vol %–fitted model prediction of the number distribution (Figure 6B), similar conclusions can be drawn, but they are much more pronounced. The model tries to predict the middle classes better compared to the lower and larger end size classes. Here, underpredictions by a factor of 10–15 occur in the classes with sizes up to 10E-6 m. Parameter estimates are such that both aggregation and breakage rates are high. In that case, all particles end up in the middle of the size range.

Because the $D[4, 3]$ is calculated based on the third and fourth moments of the distribution, it is volume related. When fitting the model to $D[4, 3]$ it can thus be expected to give results similar to those found when fitting on the volume percentage distribution, an expectation that was confirmed (Figure 6). However, the underprediction of the lower-end classes is even more severe (15–30 times). Parameter estimates are somewhat higher than those found when fitting on volume percentages (Table 2). Another noteworthy observation is that the discretized solution technique that was used here and by Biggs and Lant[13] conserves only numbers (zeroth moment) and mass (third moment). To calculate the $D[4, 3]$ the prediction of the fourth moment is needed, which is not at all guaranteed to be conserved. This is another argument why it is dangerous to use $D[4, 3]$ as a fitting variable.

Fit on N_i/Weighted N_i. When fitting on N_i, the prediction of the volume percentage distribution is poor. However, from Figure 7 one can see that the predictions of the lower-size tail are better compared to fitting either on the volume percentage distribution or on $D[4, 3]$. After a closer inspection of the prediction of the number distribution, similar observations can be made. Underprediction factors of the lower tail now range between 1.5 and 2.5, which is still rather high, but already much better compared to fitting on volume percentage distribution or $D[4, 3]$. The reason for this is the fact that when fitting to numbers, the absolute number of flocs in every class will determine which classes will contribute most to the $J(\theta)$. Because flocs are abundantly present at the lower end of the size range, these classes are highlighted during the calibration. To do so, the parameter estimates are decreased by the optimization algorithm. This means that both aggregation and breakage occur at slower rates. In the application at hand, gravitational solid–liquid separation, one is mainly interested in the small flocs that will not settle. This means that a better prediction of the small-size classes is needed. In this regard, it is better to fit the current model to the number distribution instead of the volume distribution because it gives a better prediction of the classes of interest. It is noted again that this can be different for other applications. However, the prediction of the number distribution is still not good because of a lack of flexibility. The model needs to be improved by using more appropriate aggregation and breakage kernels, although the strategy that one would follow to do so might be quite different depending on the fitting variable.

Finally, when fitting on weighted N_i using the multinomial approach to calculate the weights, results similar to those of fitting on N_i were found. However, because the calculated measurement errors are positively correlated with the absolute numbers in the size classes, they will be larger for classes containing large numbers of particles and thus their weights will be smaller. This results in lower predictions of both volume percentages and numbers in the lower and middle ranges. Underpredictions of the lower end size classes range between 2 and 3.3. Only the parameter estimate for α is slightly higher, resulting in somewhat faster aggregation, a phenomenon attributed to the fact that the contribution of the lower end class prediction to the $J(\theta)$ is reduced because these measurements are less certain, whereas the contribution of larger classes to the $J(\theta)$ has increased.

Conclusions

A new comprehensive methodology was presented that deals with problems that arise when calibrating a PBM using experimental data collected on-line during flocculation. Four issues were discussed: (1) choice of solution method, (2) data transformation, (3) measurement errors, and (4) choice of fitting variable(s).

It was shown that the fixed-pivot solution method overpredicts both the zeroth moment and the number of flocs in the large-size class range, in agreement with findings by Kumar and Ramkrishna,[33] leading to a severe underprediction of the aggregation parameter α (50%). Therefore, use of the moving-pivot technique to solve the PBM is advised.

Data transformation is required to ensure compatibility between experimental data and the model. The calculation of the volume percentage distribution in the model grid was accomplished by means of calculating the cumulative volume percentage distribution and interpolating at the pivots of the model grid. A new approach for volume-to-number conversion, based on a fixed total floc volume, was presented. The total floc volume could be calculated from the sludge concentration (X) and the densities of liquid (ρ_l), solids (ρ_s), and flocs (ρ_f). The technique conserved the $D[4, 3]$ of the original distribution.

Finally, the PBM was fitted to four different fitting variables: (1) volume percentage distribution, (2) $D[4, 3]$, (3) number distribution, and (4) weighted number distribution. Fitting on volume-based variables (vol %, $D[4, 3]$) resulted in good predictions of the volume percentage distribution. However, both tails of the distribution are underpredicted. The predictions of the number distribution showed a similar result, but more pronounced with underpredictions in the lower end up to a factor of 10–30. Parameter estimates are quite high, forcing the particles to move to the middle of the size range. Moreover, it should also be noted that the fourth moment, which is used to calculate the $D[4, 3]$, is not conserved by the discretized solution technique. Fitting on number-related variables (N_i, weighted N_i) resulted in poor overall predictions of the volume percentage distribution, although the underpredictions at the lower end tail were found to be smaller. Again, more pronounced results were found for the predictions of the number distribution. Underpredictions of the lower end size classes ranged between 1.5 and 3.3. Parameter estimates correspond to lower aggregation/breakage rates. For the application at hand, gravitational solid–liquid separation, it is advised to optimize the model by means of the number distribution and not volume distribution, noting that this might be different for other applications.

Acknowledgments

The project was financially supported by the Fund for Scientific Research–Flanders (Project No. G.0032.00) and the Ghent University Research Fund (BOF 01111001).

Notation

a = constant in breakage rate function (=1/3)
A = breakage rate coefficient, $m^{-1}\ s^{-1}$
C = ratio between liquid and solid mass
$CON(x)$ = cumulative oversize numbers
d_i = diameter of a particle in class i (= pivot diameter), m
$D[4, 3]$ = mass mean diameter, m
$\Delta F_N(x)_i$ = number fraction in size class i
$\bar{G}$ = average velocity gradient, s^{-1}
$h(x, t)$ = net aggregation rate, $m^{-3}\ s^{-1}$
$J(\theta)$ = sum of squared errors
m_l = liquid mass, kg
m_s = solid mass, kg
$n(x, t)$ = property number distribution function, # m^{-3}
N = total number of particles, # m^{-3}
N_i = number of particles in class i, # m^{-3}
$S(x)$ = breakage rate of particles of size x, s^{-1}
t = time, s
V_f = total floc volume, m^3
V_i = volume of size class i, m^3
V_T = total sample volume (solids + liquid), m^3
x = floc size expressed in volume, m^3
$\dot{X}(x, t)$ = growth rate of property x, s^{-1}
X = activated sludge concentration, kg m^{-3}

Greek letters

α = collision efficiency
$\beta(x - x', x)$ = collision frequency for particles of volume, $m^3\ s^{-1}$
$\bar{\varepsilon}$ = average turbulent energy dissipation rate, $m^2\ s^{-3}$
Γ = breakage distribution function
ρ_l = liquid density, kg m^{-3}
ρ_f = floc density, kg m^{-3}
ρ_s = dry solids density, kg m^{-3}
$\sigma^2(N_i)$ = variance of number of particles, N_i
ν = kinematic viscosity, $m^2\ s^{-1}$

Literature Cited

1. Gujer W, Henze M, Mino T, van Loosdrecht M. Activated sludge model No. 3. In: Henze M, Gujer W, Mino T, van Loosdrecht M, eds. *Activated Sludge Models ASM1, ASM2 and ASM3*. London: IWA Publishing; 2000:101-121.
2. Stamou AI, Rodi W. Numerical modeling of flow and settling in primary rectangular clarifiers. *J Hydr Res*. 1989;27:665-682.
3. Zhou S, McCorquodale JA. Modeling of rectangular settling tanks. *J Hydr Eng*. 1992;118:1391-1405.
4. Stichting Toegepast Onderzoek Waterbeheer [STOWA (Foundation on Applied Water Management Research)]. *Optimalisatie van ronde nabezinktanks: Ontwikkeling nabezinktankmodel en evaluatie STORA-ontwerprichtlijn*. Utrecht, The Netherlands: STOWA; 2002.
5. De Clercq B. *Computational Fluid Dynamics of Settling Tanks: Development of Experiments and Rheological, Settling, and Scraper Submodels*. PhD Dissertation. Ghent, Belgium: Ghent University; 2003.
6. Nopens I, Biggs CA, De Clercq B, Govoreanu R, Wilen BM, Lant PA, Vanrolleghem PA. Modelling the activated sludge flocculation process combining laser light diffraction particle sizing and population balance modelling (PBM). *Water Sci Technol*. 2002;45:41-49.
7. Parker DS Kaufman WJ, Jenkins D. Floc break-up in turbulent flocculation processes. *J Sanit Eng Pro Div Am Soc Civ Eng*. 1972;98:79-99.
8. Wahlberg EJ, Keinath TM, Parker DS. Influence of activated sludge flocculation time on secondary clarification. *Water Environ Res*. 1994;66:779-786.
9. Wilen BM. *Properties of Activated Sludge Flocs*. PhD Dissertation. Goteborg, Sweden: Chalmers University of Technology; 1999.
10. Serra T, Colomer J, Casamitjana X. Aggregation and break-up of particles in a shear flow. *J Colloid Interface Sci*. 1997;187:466-473.
11. Guan J, Waite D, Amal R. Rapid structure characterization of bacterial aggregates. *Environ Sci Technol*. 1998;32:3735-3742.
12. Waite T. Measurement and implications of floc structure in water and wastewater treatment. *Colloid Surf A Physicochem Eng Aspects*. 1999;151:27-41.
13. Biggs CA, Lant PA. Activated sludge flocculation: On-line determination of floc size and the effect of shear. *Water Res*. 2000;34:2542-2550.
14. Randolph A, Larson M. *The Theory of Particulate Processes*. New York, NY: Academic Press; 1971.
15. Spicer PT, Pratsinis SE. Coagulation and fragmentation: Universal steady state particle size distribution. *AIChE J*. 1996;42:1616-1620.
16. Blatz BJ, Tobolsky AV. Note on the kinetics of systems manifesting simultaneous polymerization–depolymerisation phenomena. *J Phys Chem*. 1945;49:77-80.
17. Manjunath S, Ghandi KS, Kumar R, Ramkrishna D. Precipitation in small systems—I. Stochastic analysis. *Chem Eng Sci*. 1994;49:1451-1463.
18. Haarhof J, Edzwald J. Modelling of floc-bubble aggregate rise rates in dissolved air flotation. *Water Sci Technol*. 2001;43:175-184.
19. Iveson S. Limitations of one-dimensional population balance models of wet granulation processes. *Powder Technol*. 2002;124:219-229.
20. Mantzaris N, Liou J, Daoutidis P, Srienc F. Numerical solution of a mass structured cell population balance model in an environment of changing substrate concentration. *J Biotechnol*. 1999;71:157-174.
21. Hidy G, Brock J. *The Dynamics of Aerocolloidal Systems*. Oxford, UK: Pergamon Press; 1970.
22. Hulburt H, Katz S. Some problems in particle technology. A statistical mechanical formulation. *Chem Eng Sci*. 1964;19:555-574.
23. Ramkrishna D. *Population Balances: Theory and Applications to Particulate Systems in Engineering*. London: Academic Press; 2000.
24. Thomas DN, Judd SJ, Fawcett N. Flocculation modelling: A review. *Water Res*. 1998;33:1579-1592.
25. Adler P. Heterocoagulation in shear flow. *J Colloid Interface Sci*. 1981;83:106-115.
26. Kusters K, Wijers J, Thoenes D. Aggregation kinetics of small particles in agitated vessels. *Chem Eng Sci*. 1997;52:107-121.
27. Ducoste J. A two-scale PBM for modeling turbulent flocculation in water treatment processes. *Chem Eng Sci*. 2002;57:2157-2168.
28. Konno M, Aoki M, Saito S. Scale effect on breakup process in liquid–liquid agitated tanks. *J Chem Eng Jpn*. 1983;16:312-319.
29. Vanni M. Approximate population balance equations for aggregation-breakage processes. *J Colloid Interface Sci*. 2000;221:143-160.
30. Kramer T, Clark M. Incorporation of aggregate breakup in the simulation of orthokinetic coagulation. *J Colloid Interface Sci*. 1999;216:116-126.
31. Hounslow MJ, Ryall RL, Marshall VR. A discretized population balance for nucleation, growth, and aggregation. *AIChE J*. 1988;34:1821-1832.
32. Kumar S, Ramkrishna D. On the solution of population balance equations by discretisation—I. A fixed pivot approach. *Chem Eng Sci*. 1996a;51:1311-1332.
33. Kumar S, Ramkrishna D. On the solution of population balance equations by discretisation—II. A moving pivot approach. *Chem Eng Sci*. 1996b;51:1333-1342.
34. Litster J, Smit D, Hounslow MJ. Adjustable discretized population balance for growth and aggregation. *AIChE J*. 1995;41:591-603.
35. Nopens I, Vanrolleghem PA. Comparison of discretisation methods to solve a population balance model of activated sludge flocculation including aggregation and breakage. Proc of IMACS 4th MATHMOD Conference, Vienna, Austria, February 5–7; 2003.
36. Govoreanu R, Seghers D, Nopens I, De Clercq B, Saveyn H, Capalozza C, Van der Meeren P, Verstraete W, Top E, Vanrolleghem PA. Linking floc structure and settling properties to activated sludge population dynamics in an SBR. Proc of 3rd IWA World Water Congress, Melbourne, Australia, April 7–12; 2002.
37. Mikkelsen L, Gotfredsen A, Agerbaek M, Nielsen P, Keiding K. Effects of colloidal stability on clarification and dewatering of activated sludge. *Water Sci Technol*. 1996;34:449-457.
38. Dochain D, Vanrolleghem PA. *Modelling and Estimation in Wastewater Treatment Processes*. London: IWA Publishing; 2001.

39. Nelder JA, Mead R. A simplex method for function minimalization. *Comput J*. 1965;7:308-313.
40. Li D, Ganczarczyk J. Size distribution of activated sludge flocs. *Res J Water Pollut Control Fed.* 1991;63:806-814.
41. Biggs CA. *Activated Sludge Flocculation: Investigating the Effect of Shear Rate and Cation Concentration on Flocculation Dynamics*. PhD Dissertation. Brisbane, Australia: University of Queensland; 2000.
42. Kinnear D. *Biological Solids Sedimentation: A Model Incorporating Fundamental Settling Parameters*. PhD dissertation. Salt Lake City, UT: University of Utah; 2002.
43. Dammel E, Schroeder E. Density of activated sludge flocs. *Water Res*. 1991;25:841-846.
44. Agresti A. *Categorical Data Analysis*. New York, NY: Wiley; 1990.

Manuscript received Feb. 23, 2004, and revision received Sept. 8, 2004.